Bondpseudorotation, Jahn-Teller, and Pseudo-Jahn-Teller Effects in the Cyclopentadienyl Cation and its Pentahalogeno Derivatives

Wenli Zou, Michael Filatov, and Dieter Cremer*

Multireference averaged quadratic coupled cluster (MRAQCC) (4,5)/cc-pVTZ calculations predict that bond pseudorotation (BPR) in the first excited singlet state of the cyclopentadienyl cation (CPC) proceeds with a barrier of just 0.35 kcal/mol, where five dienylic forms present the minima and five allylic forms the transition states of the pseudorotation process. Vibrational and entropic corrections revert the order of stabilities and lead to a $\Delta G(298)$ of just 0.05 kcal/mol indicating that BPR is unhindered at room temperature. The description of the CPC ring in terms of curvilinear deformation coordinates (seven for C_5, seven for X_5, and three coupling coordinates) make it possible to explore both the six-dimensional (6D) Jahn-Teller and the 8D pseudo-Jahn-Teller space and assess the importance of Jahn–Teller and pseudo-Jahn–Teller deformations of the CPC ring. The latter dominate the ring deformations along the BPR path. The only somewhat larger Jahn–Teller contribution results from a E_1'-symmetrical CCH bending motion. For the perhalogenated CPCs, the dominance of the pseudo-Jahn–Teller effect increases, however, the total deformation of the D_{5h}-symmetrical ring decreases and thereby also the stabilization of the $^1A_1$ forms along the BPR path. This leads to a reduction of the BPR barriers to just 0.14 kcal/mol for $C_5I_5^+$. For all pentahalogeno CPCs, the dienylic form is more stable both at the energy and free energy level. The use of curvilinear deformation coordinates facilitates the understanding of the electronic features of cyclic (pseudo-) Jahn–Teller systems. © 2012 Wiley Periodicals, Inc.

DOI: 10.1002/qua.24116

Introduction

Bond pseudorotation (BPR) is an internal molecular rearrangement process of cyclic Jahn–Teller systems, which is little understood due to inherent difficulties to obtain detailed experimental descriptions.[1–5] During BPR, the bonds of a planar molecule are cyclically shifted along the perimeter of a ring molecule thus presenting a rotation of the peripheral bonds around the center of the ring. This process will preferentially take place if a high-symmetry ring form undergoes a Jahn–Teller or pseudo-Jahn–Teller distortion of E-type symmetry. We have recently introduced a set of curvilinear deformation coordinates, which span a 1- and N-2 two-dimensional (2D) subspaces of the total deformation space of a planar regular N-membered ring ("N-gon") and which are associated with the *A*-symmetrical breathing and the *E*-symmetrical pseudorotation motions of an N-gon.[5] The latter can be viewed as if the atoms of the N-gon carry out in-phase and in-plane rotations around the corners of the N-gon, which lead to a periodic deformation of the ring without producing an angular momentum. Alternatively, one can consider this dynamic process as a rotation of the E-symmetrical ring deformation around its origin. We call this internal movement of a ring an elementary BPR motion.

The actual BPR of an N-ring can be identical with the *n*th elementary BPR process described by curvilinear (cylindrical) coordinates t_n (BPR amplitude) and τ_n (BPR phase angle with $0 \leq \tau \leq 360°$)[5] or a linear combination of elementary BPR processes as it is the case for *N* being odd. In this work, BPR of the cyclopentadienyl cation (CPC, $N = 5$, **1**), $C_5H_5^+$, and its perhalogenated derivatives is investigated ($C_5X_5^+$, X = F, Cl, Br, I; **2–5**, Fig. 1) and the relevance of its three ($n = 1, 2, 3$) elementary BPR processes (see Fig. 2) for electronic structure and dynamic behavior is analyzed. The three BPR motions lead in some combination to the actual BPR of CPC shown in Fig. 3, and we will quantitatively determine their contributions.

CPC has been the target of several experimental investigations,[6–9] which because of its peculiar electronic structure and chemical behavior triggered extended computational studies.[9–14] CPC was identified in the mass spectrum[15,16] and its solvolytic generation was reported by Tidwell and coworkers,[17] who also summarized the early synthetic work on CPC. The ground state of CPC was identified to be a triplet with D_{5h}-symmetry ($\tilde{X}^3A_2'$) and the adiabatic singlet–triplet splitting was determined to be 4.38 kcal/mol.[9] Special focus was laid on the description of the first excited singlet state of **1**, which according to electronic structure theory should be an antiaromatic D_{5h}-symmetrical $^1E_2'$ state with 4π electrons (**1c**, Fig. 1). A possible Jahn–Teller distortion of this state was discussed at an early stage where a summary of the early theoretical work on CPC can be found in the book by Bersuker.[3]

Recently, a detailed pulsed-field-ionization zero-kinetic-energy (PFI-ZEKE) photoelectron spectroscopy study of $C_5H_5^+$ and $C_5D_5^+$

W. Zou, D. Cremer
Department of Chemistry, Southern Methodist University, 3215 Daniel Ave, Dallas, Texas 75275-0314
E-mail: dieter.cremer@gmail.com

Contract grant sponsor: National Science Foundation; Contract grant number: CHE 071893.

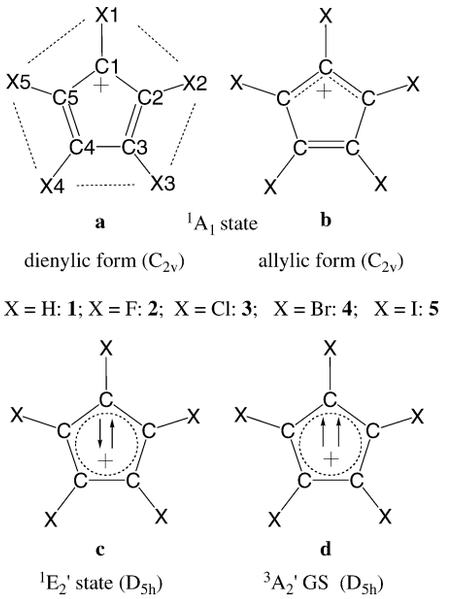

Figure 1. Dienylic form **1a** and allylic form **1b** of the $^1A_1$-state, the $^1E_2'$ excited state **1c**, and the $\tilde{X}^3A_2'$ ground state of unsubstituted and pentahalogeno CPCs, $C_5X_5^+$. Antiparallel and parallel arrows indicate a singlet and triplet state, respectively. The virtual ring formed by the five substituents X is indicated by dashed lines for **1a**.

was carried out by Wörner and Merkt.[9] These authors also analyzed the vibronic coupling of the D_{5h}-symmetrical $^1E_2'$ state and found that the deformations of the molecule are caused by a pseudo-Jahn–Teller effect (PJTE) rather than a Jahn–Teller effect (JTE),[9] which was first predicted by Borden and Davidsson.[12]

In this work, we will demonstrate how the results of the time-consuming and complicated vibronic coupling analysis of **1c** can be predicted by optimizing the geometry of CPC forms along the BPR path in terms of curvilinear deformation coordinates.[5] The latter account for all A-, B-, and E-symmetrical ring deformations of the D_{5h}-symmetrical five-membered ring ("5-gon"), and therefore, we will be able to quantitatively assess the electronic importance of the three elementary deformation processes for the actual BPR of CPCs. The results of this investigation will be presented as follows. In Computational Methods Section, the major steps of deriving curvilinear deformation coordinates will be sketched and the computational methods used will be described. In Results and Discussion Section, results are presented and discussed. Conclusions Section summarizes the conclusions of this work.

Computational Methods

For the purpose of deriving the relevant deformations of $C_5X_5^+$, we specify that the CPC molecule is located in the x, y-plane with the z-axis being the normal to this plane. The origin of the coordinate system is identical with the geometrical center of the CPC ring. Atom C1 is positioned on the $-x$-axis and the ring atoms are numbered clockwise. The substituent atom X1 is bonded to C1, X2 to C2, and so forth (see Fig. 1a). In this way, the ring standard orientation is defined.

The derivation of deformation coordinates is based on a characterization of the inplane motions of an N-ring with the help of the vibrational modes of the corresponding N-gon. In the case of a pentagon, there are 15 motions, which are characterized according to their symmetry using the D_{5h} point group (see Table 1). Three translational motions T_x, T_y, (both of E_1' symmetry; Table 1), T_z (A_2'') and three rotational motions of the ring R_x, R_y, (both of E_1'' symmetry), R_z (A_2') can be excluded from the analysis. The A_1'-symmetrical breathing motion of the pentagon preserves the D_{5h} symmetry of the ring, however, leads to a change in its side lengths, that is, CC bond lengths. We specify a breathing parameter R_0, which is equal to the radius of the circumscribed circle (CC bond lengths = $2\ \sin(\frac{\pi}{N})R_0 = 1.1756\ R_0$ for $N = 5$) of the C_5-pentagon representing the minimum energy form of the $^1E''$ state of CPC. A deformation of this pentagon can lead to a new value of R and we call $t_0 = R - R_0$ the amplitude of the breathing deformation of the C_5-pentagon.

There are one E_1'-symmetrical and two E_2'-symmetrical deformation modes corresponding to elementary BPR modes with $n = 1, 2, 3$ (Table 1). These are associated with the corresponding vibrational modes of a D_{5h}-symmetrical ring molecule (see also Fig. 2). The curvilinear coordinates describing these deformations are t_n and τ_n, where the first is the amplitude of deformation and the latter the phase angle of deformation. This leads to a set of four deformation amplitudes and three phase angles, which are sufficient for generating all possible inplane deformations of the 5-gon. For a nonplanar ring, they would be complemented by a pair of puckering coordinates (amplitude q_2 and phase angle ϕ_2[18–20]) specifying the puckering of the 5-gon.

With the help of the character table of an N-gon one can show that the number of unique inplane deformation pairs is always $N-2$ so that $2(N-2)+1 = 2N-3$ (= 7 for $N = 5$) coordinates (including the breathing deformation) define the deformed N-gon. The derivation of suitable curvilinear coordinates (rather than internal coordinates) has been described elsewhere.[5] Here, we will just outline the major idea of this derivation, where special emphasis is laid on the inclusion of suitable curvilinear coordinates for substituents X of $C_5X_5^+$ into the deformation analysis.

Each inplane deformation of the 5-gon is given by a set of five deformation vectors $\mathbf{d}_k$ ($k = 0, \ldots, 4$), which define the new positions of the five atoms C_k in the deformed ring. Each deformation vector can be expressed in terms of the unit vectors $\mathbf{i}_k$ and $\mathbf{j}_k$ in x and y-direction of the coordinate system thus yielding

$$\mathbf{d}_k = x_k\mathbf{i}_k + y_k\mathbf{j}_k \tag{1}$$

at atom C_k of the ring. As there are four different contributions $n = 0, 1, 2, 3$ (including the breathing deformation) to a deformation vector $\mathbf{d}_k$ and only the first one with $n = 0$ is exclusively a radial one, the orientations of the three remaining ones have to be determined with the help of the rotation angles $\omega_k^{(n)}$ specified by the D_{5h} point group character table:

$$\omega_k^{(n)} = \frac{2\pi(n+1)k}{N} \tag{2}$$

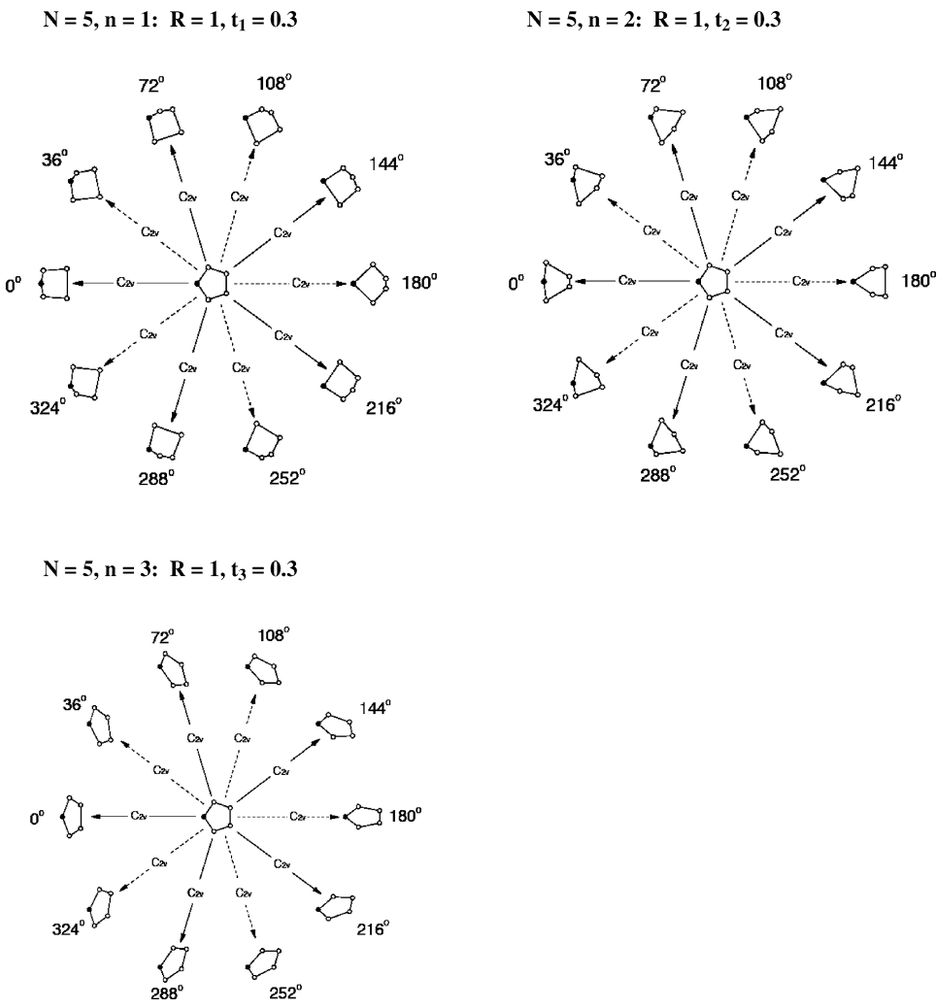

Figure 2. Elementary bondpseudorotation (BPR) processes taking place in the 2D spaces spanned by curvilinear coordinate pairs $\{t_1, \tau_1\}$, $\{t_2, \tau_2\}$, and $\{t_3, \tau_3\}$. Deformation mode $n = 1$ leads to the impression of a four-ring, $n = 2$ to a three-ring, and $n = 3$ to a *two-ring* (circle). In this order, the deformation of the five-ring becomes more delocalized. The deformed ring forms are shown for a fixed value of t_n and pseudorotation phase angle τ_n increasing from 0 to 360°. The position of atom 1 is indicated by a black dot (clockwise numbering of ring atoms). Only the ten C_{2v}-symmetrical forms along the BPR path surrounding the undeformed D_{5h} form of the five-ring are shown.

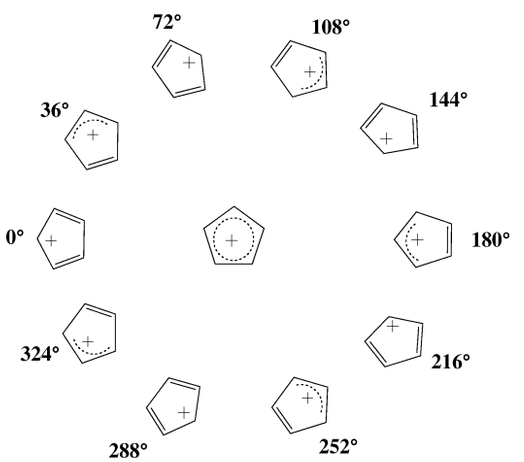

Figure 3. BPR of the CPC. Only the five C_{2v}-symmetrical dienylic forms at 0, 72, 144, 216, and 288° and the five C_{2v}-symetrical allylic forms at 36, 108, 180, 252, and 324° are shown. There is an infinite number of C_s-symetrical CPC forms along the BPR path.

where $n = 0, \ldots, N-2$ ($N = 5$ for CPCs). The unit vectors are defined according to

$$\mathbf{i}_k^{(n)} = \mathbf{i}_k \cos\omega_k^{(n)} - \mathbf{j}_k \sin\omega_k^{(n)} \quad (3a)$$

$$\mathbf{j}_k^{(n)} = \mathbf{i}_k \sin\omega_k^{(n)} + \mathbf{j}_k \cos\omega_k^{(n)} \quad (3b)$$

which gives for the deformation vectors of the *N*-gon:

$$\mathbf{d}_k = \sum_{n=0}^{N-2} \left[x_k \mathbf{i}_k^{(n)} + y_k \mathbf{j}_k^{(n)} \right] \quad (4)$$

It is desirable to convert Eq. (4) with the help of a Fourier transformation into form (5):

$$\mathbf{d}_k = \sum_{n=0}^{N-2} \left[A_n \mathbf{i}_k^{(n)} + B_n \mathbf{j}_k^{(n)} \right] \quad (5)$$

Table 1. Number and character of the normal vibrations of each irreducible representation of the D_{5h} point group given for the C_5 ring frame and the X_5 substituent frame of a cyclopentadienyl cation $C_5X_5^+$.[a]

Irrep	N_{C5}	Char	N_{X5}	N_{coup}	N_{C5X5}	Comment
A_1'	1	Breathing	1	0	2	Breathing
A_1''	0	–	0	0	0	–
A_2'	0	R_z (ip)	0	1	1	Coupling $\{R_z, R_z\}$(ip)
A_2''	0	T_z(oop)	0	1	1	Coupling $\{T_z, T_z\}$(oop)
E_1'	0	T_x, T_y (ip)	0	1	3	Coupling $\{T_x, T_x\}\{T_y, T_y\}$ (ip)
	1	deform $n = 1$ (ip)	1			all 3 contribute to JTE (ip)
E_1''	0	R_x, R_y (oop)	0	1	1	Coupling $\{R_x, R_x\}\{R_y, R_y\}$ (oop)
E_2'	2	deform $n = 2, 3$ (ip)	2	0	4	all 4 contribute to PJTE (ip)
E_2''	1	deform $m = 2$ (oop)	1	0	2	puckering (oop)
Sum	9		9	3 + 3	24	3 ip + 3 oop couplings

[a] Irrep: Irreducible representation; N_{C5}: number of vibrations of the C_5 ring frame; N_{X5}: number of vibrations of the X_5 substituent frame ("virtual X_5 ring"); N_{coup}: number of coupling vibrations between the C_5 and X_5 frames; $N_{C5X5} = N_{C5} + N_{X5} + N_{coup}$: total number of vibrations of the C_5X_5 molecule; Char: characterization of in-plane (ip) and out-of-plane (oop) motions including translations (T), rotations (R), and ip/oop-deformations (deform); counting of ip-deform starts with $n = 1$, that of oop-deform with $m = 2$;[18] in the last column the coupling vibrations between the C_5 and X_5 frames are given in short form as explained in the text; also indicated are the deformation vibrations, which lead to a JTE or pseudo-Jahn–Teller effect (PJTE).

where the Fourier coefficients A_n and B_n are given by

$$A_n = \frac{1}{N}\sum_{k=0}^{N-1}\left[x_k \cos\omega_k^{(n)} - y_k \sin\omega_k^{(n)}\right] \quad (6a)$$

$$B_n = \frac{1}{N}\sum_{k=0}^{N-1}\left[x_k \sin\omega_k^{(n)} + y_k \cos\omega_k^{(n)}\right] \quad (6b)$$

This has the advantage that all deformation vectors adopt the same length and are in phase. Furthermore, the Fourier coefficients can be used to derive curvilinear coordinates t_n and τ_n:

$$t_n^2 = A_n^2 + B_n^2 \quad (7a)$$

$$\tau_n = \arctan(B_n/A_n) \quad (7b)$$

for $n = 1, 2, 3$ and $R^2 = A_0^2 + B_0^2$ for $n = 0$ with t_0 as defined above. In this way, the contribution to the deformation vector in mode n is given by

$$\mathbf{d}^{(n)} = t_n\ [\cos\ \ \tau_n\ \mathbf{i}^{(n)} + \sin\ \ \tau_n\ \mathbf{j}^{(n)}] \quad (8)$$

where all contributions $\mathbf{d}_k^{(n)}$ to $\mathbf{d}^{(n)}$ have the length t_n and sum up to zero:

$$\sum_{k=0}^{N-1}\mathbf{d}_k^{(n)} = 0 \quad (9)$$

The total deformation amplitude T is obtained from

$$T^2 = \sum_{n=0}^{N-2} t_n^2 = \sum_{n=0}^{N-2}\left[A_n^2 + B_n^2\right] = \frac{1}{N}\sum_{n=0}^{N-2}\left[x_n^2 + y_n^2\right] \quad (10)$$

The total deformation amplitude T can be used to determine the contribution of each deformation mode n to the total ring deformation (given in percentage) using the ratio t_n^2/T^2. In the following, we will see that this is useful for identifying the influence of different physical effects on the electronic structure of the ring molecule.

The 2N-3 curvilinear coordinates (of the hypercylindrical type) obtained to describe the geometry of the C_5 ring can be extended to describe also the positions of the substituents X. For the purpose of facilitating the derivation, we consider first a virtual X_5 ring. As indicated in Table 1, there are again an A_1' symmetrical breathing mode and three E_1' or E_2'-symmetrical deformation modes where all these can be considered to effect just the virtual X_5 ring. In this way, seven curvilinear substituent (S) coordinates $\{t_0^S; t_1^S, \tau_1^S; t_2^S, \tau_2^S; t_3^S, \tau_3^S\}$ are defined for the ring substituents. This leads to a total of 14 coordinates, whereas the correct number of coordinates to describe planar $C_5X_5^+$ is 17. The three remaining coordinates represent the coupling between the C_5 and the X_5 ring.

The first coupling term is derived from the A_2'-symmetrical inplane rotation of C_5, which is counteracted by a rotation of the virtual X_5 ring in the opposite direction (R_z, R_z coupling, Table 1). In this way, all CCX bond angles are distorted in the same way, which can be measured by an angle $\Delta\alpha^S$. This coordinate reflects the difference in the magnitudes of the opposite rotation vectors. Any $\Delta\alpha^S < 0$ will reduce the symmetry of $C_5X_5^+$ to C_s.

The two remaining couplings between the C_5 and the X_5 ring result from opposite translations of C and X atoms in either the x- (T_x) or y-direction (T_y). These two movements may be in-phase or out-of-phase, thus, requiring for their description amplitude differences Δt_x and / or Δt_y. It is convenient to proceed as in the case of the ring deformation coordinates and to describe the translational coupling by the two cylindrical coordinates Δt^S and $\Delta\tau^S$, where the latter coordinate gives the phase-relationship between the two coupled in-plane movements of the C_5 and the X_5 ring.

Table 1 reveals that for a nonplanar ring there are additional three coupling constraints between the C_5 and the X_5 ring, which concern an A_2''-symmetrical coupled translation along the z-axis (T_z). This can be assessed by a parameters Δq^S (difference in translational displacements q_1 and q_1^S for inner and outer ring). Finally, there is the E_1''-symmetrical coupling between the R_x and the R_y modes for inner and outer ring (Table 1), which in the same spirit as done for the transformations T_x and T_y,

can be determined by a coordinate pair $\Delta\beta^S$ and $\Delta\phi^S$ (differences in rotational vectors and phase difference between the two rotations R_x, R_x and R_y, R_y; Table 1). It can be easily shown that for a ring molecule Y_NZ_N with arbitrary N, there are just six coupling vibrations leading to six coupling deformation coordinates: $(3 \times 2N - 6) - (3N - 3) - (3N - 3) = 6$, of which three describe the in-plane deformation coupling and three the out-of-plane puckering coupling between the Y_N and the virtual Z_N ring.

If just the C_{2v}-symmetrical CPC forms are considered, all deformation phase angles are fixed, and four deformation amplitudes t_n ($n = 0, 1, 2, 3$) are sufficient to determine the geometry of the C_5-ring. Similarly, for the positions of the five X atoms just t_n^S ($n = 0, 1, 2, 3$) and Δt^S for the translational coupling mode are required. (The coupling angles $\Delta\alpha^S$ and $\Delta\tau^s$ must be equal to zero because of symmetry reasons.) For the optimized geometries of C_{2v}-deformed CPC molecules, both t_0, t_0^S, and Δt are small (see below) where the smallest contribution (Δt) is not discussed in this work.

In previous work, we developed algorithms that convert Cartesian coordinates and internal coordinates into curvilinear coordinates and vice versa.[5] Programs have been written to carry out geometry optimizations and frequency calculations in terms of curvilinear coordinates without ever referring to bond lengths or bond angles.[21] All calculations based on curvilinear coordinates and presented in this work have been carried out with the program RING,[22] which is a part of the ab initio program COLOGNE11.[23]

The quantum chemical calculations were performed with the ab initio program packages COLOGNE11,[23] CFOUR,[24] and MOLPRO.[25] Because of the multireference character of the D_{5h}-symmetrical CPC form **1c** (Fig. 1) a full set of calculations was carried out using multireference averaged quadratic coupled cluster (MRAQCC) theory[26] using all single and double excitations and numerical gradients. The active space included the 4π electrons and the five lowest π MOs of a_2'', e_1'', and e_2'' symmetry. This led to a reliable description of the single–triplet excitation energy and the energy of the $^1E_2'$ state of CPC in relation to its (pseudo-)Jahn–Teller relaxed BPR forms. The latter are no longer multireference systems although the correct description of BPR in any CPC molecule is a challenging task because of the small energy differences, which have to be determined. Therefore, a number of different ab initio and density functional theory (DFT) methods was applied to test the accuracy of the different approaches and to obtain reliable descriptors for the BPR process. The methods used include CCSD(T) (coupled cluster theory with all single (S) and double (D) excitations and a perturbative treatment of all triple (T) excitations),[27] state-averaged CASSCF(4,5),[28,29] and state-averaged CASPT2(4,5)[30] (averaging was done over the lowest two $^1A_1$ and the lowest $^1B_2$ state: CASSCF(4,5)-3 or just over the lowest $^1A_1$ and $^1B_2$ state: CASSCF(4,5)-2; the same notations were used for MRAQCC and CASPT2). In addition, seven different XC-functionals were used: the hybrid functionals B3LYP[31,32] and PBE0,[33] the meta GGA hybrid functionals M06[34] and TPSSh,[35] the range-separated hybrid functionals CAM-B3LYP[36] and HSE06,[37] the double hybrid functional B2PLYP.[38]

DFT calculations of the $^1E_2'$ state were carried out using multideterminant DFT at the restricted ensemble Kohn–Sham (REKS)[39,40] level of theory with an active (2,2) space spanned by the e_1'' π MOs. A small perturbation of the D_{5h}-symmetrical $^1E_2'$ state significantly reduces the multireference character of CPC ions so that single-determinant DFT descriptions, which always include also some nondynamic electron correlation,[41–43] can be applied to get reasonable geometries and vibrational frequencies.

All calculations were carried out with the cc-pVTZ basis set.[44] In the case of Br and I, the SDB-cc-pVTZ basis set of Martin and Sundermann[45] in combination with the corresponding relativistic effective core potentials of Bergner et al.[46] were used.

Geometry optimizations and frequency calculations were based on the use of curvilinear coordinates, that is, the geometry optimization was carried out in terms of deformation coordinates rather than internal coordinates.[21] For the calculation of the deformation surface, 26 CPC ring forms, preferentially along the BPR path, were calculated, which implied the optimization of 17 deformation parameters in the case of the C_s-symmetrical ring forms. We note that the calculation of the energy at a given point of the deformation surface requires that an amplitude t_n and a phase angle τ_n are fixed at specific values and the 15 remaining curvilinear coordinates are optimized. This cannot be done using Cartesian or internal coordinates because, for example, fixing of two internal coordinates does not specify a particular deformation. Any such deformation leads to five specific bond lengths and five specific bond angles, which cannot be determined by two internal coordinates, but by two deformation coordinates.

For the MRAQCC(4,5)-3 calculations, harmonic vibrational frequencies were determined at the CASPT2(4,5)-3 level of theory to obtain zero-point-energy (ZPE), thermochemical, and entropy (S) corrections. For all other methods, the same level of theory was used for energy determination, geometry optimization, and frequency calculations, however, with the exception of the REKS(2,2)/B3LYP calculations of the $^1E_2'$ state.

The potential energy function of the deformation surface was expressed as truncated power series in deformation amplitudes t_n and Fourier expansions in the phase angles τ_n:

$$\begin{aligned} V(t_1,t_2,t_3,\tau_1,\tau_2,\tau_3) = V_0 &+ V_{2000}t_1^2 + V_{4000}t_1^4 + V_{0200}t_2^2 + V_{0400}t_2^4 \\ &+ V_{0020}t_3^2 + V_{0040}t_3^4 + V_{2200}t_1^2t_2^2 + V_{2020}t_1^2t_3^2 \\ &+ V_{0220}t_2^2t_3^2 + V_{1005}t_1\cos 5\tau_1 \\ &+ V_{0105}t_2\cos 5\tau_2 + V_{0015}t_3\cos 5\tau_3 \end{aligned} \quad (11)$$

where V_0 is the energy of the D_{5h}-symmetrical form and the dependence on R has been dropped because in all cases investigated t_0 is small with changes $\leq 1 \times 10^{-3}$ Å. The subscripts of the potential coefficients V indicate (in the first three positions), the value of n by position (t_1: position 1, etc.), the power of t_n by giving the relevant exponent, and (in fourth position) the multiplicity m of the potential via $cos\ m\ \tau_n$. For example, V_{2005} is the coefficient of the term $t_1^2\ cos\ 5\tau_1$. The flatness of the potential along the BPR path did not require quadratic or quartic amplitude terms in combination with cos terms.

Table 2. MRAQCC(4,5)-3/cc-pVTZ results for $C_5H_5^+$.[a]

State	Sym.	Comment	ΔE	ZPE	$\Delta H(298)$	$\Delta G(298)$	S	R	R^S	T	T^S	CC	CH
$\tilde{X}^3A_2'$	D_{5h}	Ground state	−6.89	50.96	−5.80	−4.54	64.02	1.2103	2.2881	0.0000	0.0000	1.4228	1.0778
$^1E_2'$	D_{5h}	1st excited state	7.46	48.83	6.82	8.31	62.28	1.2130	2.2907	0.0000	0.0000	1.4260	1.0777
$^1A_1$	C_{2v}	TS of BPR	0.35	49.06	0.00	0.00	67.29	1.2177	2.2953	0.0566	0.0352	1.4316	1.0781
$^1A_1$	C_{2v}	Min of BPR	0.00	49.55	0.34	0.05	68.26	1.2169	2.2944	0.0654	0.0411	1.4310	1.0782

[a] Energy values in kcal/mol relative to the minimum (Min) of the BPR surface; entropy S in entropy units; breathing radii R and R^S, total deformation amplitudes T and T^S, CC, and CH bond lengths all in Å. In the case of C_{2v}-symmetry, average CC and CH bond lengths are given.

Results and Discussions

In Tables 2 and 3, calculated MRAQCC(4,5) energies ΔE, ZPE, entropy S, $\Delta H(298)$, and $\Delta G(298)$ values of CPC **1** (Fig. 1) and geometries expressed both in deformation and internal coordinates are listed. Table 3 also gives energies and geometries of BPR forms calculated with CASPT2, CASSCF, and various DFT approaches. In addition, the B3LYP results for the corresponding perhalogenated CPCs **2**–**5** are listed. The corresponding energies, enthalpies, entropies, and free energies are summarized in Table 4. Figures 4a and 4b give contourline diagrams and perspective drawings of the deformation surface of CPC **1** (X = H) in the $\{t_3, \tau_3\}$-space, Figure 5 depicts the calculated B3LYP/cc-pVTZ energy and free energy potentials $V(t_3, \tau_3)$ along the BPR path for CPCs **1** – **5**.

The calculated MRAQCC(4,5) singlet–triplet splitting between the D_{5h}-symmetrical $\tilde{X}^3A_2'$ ground state and the D_{5h}-symmetrical $^1E_2'$ (pseudo-)Jahn–Teller unstable first excited state is 14.35 kcal/mol (Table 2). This value is 1.6 kcal/mol lower than given by a recent CASSCF(4,5) calculation.[9] We note in this connection that the calculation of the $^1E_2'$ state (Fig. 1) is difficult because of its multireference character and the necessity of including a sufficient amount of dynamic electron correlation where the infinite order effects of the coupled cluster theory lead to some guarantee that nondynamic and dynamic correlation effects are accounted for in a balanced way. Both CASSCF and CASPT2 cannot provide such a balanced description because of the lack of dynamic correlation or its limitation to pair correlation effects. This is reflected by the CASCF(4,5) and CASPT2(4,5) results obtained in this work, which vary over a range of 10 kcal/mol from 12 to 22 kcal/mol where the fact that the better method (CASPT2, 22 kcal/mol) leads to the larger deviation from the MRAQCC values reveals the shortcoming of a CAS approach in this case. Similarly flawed are the DFT descriptions of **1c**. For example, with REKS(2,2)/B3LYP/cc-pVTZ a singlet–triplet excitation energy of 16.3 kcal/mol (Table 4) is calculated, whereas the corresponding RB3LYP value is 26.1 kcal/mol. However, a tiny deformation of the D_{5h}-symmetrical $^1E_2'$ state lowers the RB3LYP value below 20 kcal/mol.

The energy difference between the most stable $^1A_1$ form with the dienyclic structure (**1a**, Fig. 1) and the $\tilde{X}^3A_2'$ ground state is just 6.9 kcal/mol at MRAQCC(4,5)/cc-pVTZ (Table 2). ZPE and temperature corrections reduce this value to $\Delta H(298) =$ 5.8 kcal/mol, which is further reduced to 4.54 kcal/mol due to the lower entropy S in the ground state. This agrees perfectly with the corresponding experimental value of 4.38 kcal/mol.[9] The $^1E_2'$-$\tilde{X}^3A_2'$ singlet–triplet splitting $\Delta G(298)$ is calculated to be 12.8 kcal/mol.

For the reasons described above, a reliable account of the deformation stabilization (this can be of the 1D *A*,*B*-symmetrical or the 2D Jahn–Teller/pseudo-Jahn–Teller type) of the $^1E_2'$ state can only be expected from the MRAQCC(4,5) description, which predicts a stabilization energy of 7.46 kcal/mol, that is, a $^1A_1$ state of CPC. The dienylic structure of **1a** (distortion from D_{5h} to C_{2v} symmetry, Fig. 1) represents the energy minimum of the singlet surface of the first excited state, whereas the allylic form **1b** is located 0.35 kcal/mol above the minimum at a first-order transition state (TS) of the surface. In view of the five-fold multiplicity of the BPR surface and the equivalence of all five minima and TSs (see Figs. 3 and 4), MRAQCC(4,5) describes CPC **1a** as a slightly hindered bond pseudorotor.

It is interesting to note that the ZPE corrections calculated at the CASPT2(4,5)-3 level of theory revert the order of stabilities so that the allylic form becomes 0.14 kcal/mol more stable, which increases to 0.40 kcal/mol at $\Delta H(298)$. Entropic contributions are larger for **1a** (Table 2) so that the $\Delta G(298)$ value is just 0.05 kcal/mol (Table 2) slightly favoring the allylic form **1b**. These values can change when using an even larger basis set and, especially, when including anharmonic corrections to the vibrational frequencies, which will also influence ZPE, S, $\Delta H(298)$, and $\Delta G(298)$ values. In any case, the MRAQCC results clarify that BPR is unhindered at room temperature in view of an RT value of 0.6 kcal/mol. Hence, CPC ion **1** is a molecule without a defined ring structure: The 5 C nuclei rotate rapidly in regions of large electron density, however, these rotations are synchronized in a way that structural changes in form of BSR move like a wave around the periphery of the ring.

As already observed in the case of the singlet–triplet splitting, CASSCF, CASPT2, CCSD(T), and DFT energies of the deformation stabilization of the D_{5h}-symmetrical $^1E_2'$ state are unreliable, either exaggerating this electronic effect (e.g., B3LYP: 15.6; CCSD(T): 13.0; CASSCF(4,5)-2: 9.9 kcal/mol) or underestimating it (CASSCF(4,5)-3: 5.7; CASPT2(4,5)-3: 1.3 kcal/mol). In addition to the fact that the $^1E_2'$ state is only reliably described by MRAQCC and that this method becomes too expensive for perhalogenated CPCs, it has to be mentioned that the location of this state on the singlet surface is the location of a primary conical intersection that is surrounded by five secondary conical intersections in connection with a $^1B_2$ state.[14] Because the correct description of this surface region and the states located therein implies a careful vibronic coupling analysis,[47] which is beyond the scope of this investigation, we will focus in the following on the BPR

Table 3. Ab initio and DFT results for the stationary points of the BPR surface of $C_5X_5^+$.[a]

No	X	Method	Form	ΔE	R R^S	T T^S	t_0 t_0^S	t_1 t_1^S	t_2 t_2^S	t_3 t_3^S	τ_1 τ_1^S	τ_2 τ_2^S	τ_3 τ_3^S	C1C2 C1X1	C2C3 C2X2	C3C4 C3X3
1	H	MRAQCC	Min	0	1.2169	0.0654	0.0039(0.4)	0.0136(4.3)	0.0159(5.9)	0.0618(89.4)	0	180	0	1.442	1.355	1.559
					2.2944	0.0411	0.0037(0.8)	0.0233(32.1)	0.0080(3.8)	0.0327(63.3)	0	0	0	1.084	1.075	1.078
			TS	0.35	1.2177	0.0566	0.0047(0.7)	0.0095(2.8)	0.0252(19.8)	0.0496(76.7)	0	0	180	1.384	1.523	1.344
					2.2953	0.0352	0.0046(1.7)	0.0197(31.2)	0.0074(4.4)	0.0279(62.7)	0	0	180	1.076	1.082	1.076
		CASPT2	Min	0	1.2168	0.0587	0.0042(0.5)	0.0125(4.5)	0.0165(7.9)	0.0548(87.1)	0	180	0	1.441	1.360	1.550
					2.2950	0.0369	0.0035(0.9)	0.0226(37.6)	0.0059(2.6)	0.0283(58.9)	0	0	0	1.084	1.077	1.079
			TS	0.29	1.2164	0.0568	0.0038(0.4)	0.0057(1.0)	0.0155(7.5)	0.0542(91.1)	0	0	180	1.393	1.509	1.347
					2.2947	0.0324	0.0032(1.0)	0.0150(21.4)	0.0070(4.7)	0.0277(73.0)	0	180	180	1.077	1.082	1.076
		CASSCF	Min	0	1.2100	0.0576	0.0030(0.3)	0.0139(5.8)	0.0148(6.6)	0.0538(87.3)	0	180	0	1.430	1.357	1.540
					2.2796	0.0387	0.0027(0.5)	0.0248(41.1)	0.0059(2.3)	0.0290(56.1)	0	0	0	1.076	1.068	1.070
			TS	0.35	1.2096	0.0555	0.0026(0.2)	0.0064(1.3)	0.0135(5.9)	0.0534(92.5)	0	0	180	1.385	1.498	1.346
					2.2792	0.0336	0.0024(0.5)	0.0167(24.6)	0.0076(5.1)	0.0281(69.8)	0	180	180	1.069	1.074	1.067
		B3LYP	Min	0	1.2153	0.0698	0.0056(0.6)	0.0135(3.7)	0.0214(9.4)	0.0648(86.2)	0	180	0	1.445	1.342	1.571
					2.2945	0.0417	0.0056(1.8)	0.0216(26.8)	0.0035(0.7)	0.0351(70.7)	0	0	0	1.085	1.077	1.080
			TS	0.54	1.2149	0.0676	0.0052(0.6)	0.0055(0.7)	0.0200(8.8)	0.0641(90.0)	0	0	180	1.385	1.523	1.325
					2.2940	0.0369	0.0051(1.9)	0.0125(11.4)	0.0052(2.0)	0.0340(84.7)	0	180	180	1.077	1.084	1.077
		PBE0	Min	0	1.2118	0.0692	0.0052(0.6)	0.0127(3.4)	0.0195(7.9)	0.0650(88.1)	0	180	0	1.441	1.340	1.562
					2.2929	0.0410	0.0051(1.5)	0.0203(24.5)	0.0055(1.8)	0.0348(72.1)	0	0	0	1.088	1.078	1.082
			TS	0.48	1.2114	0.0673	0.0048(0.5)	0.0053(0.6)	0.0183(7.4)	0.0644(91.5)	0	0	180	1.382	1.517	1.324
					2.2926	0.0368	0.0048(1.7)	0.0120(10.6)	0.0069(3.5)	0.0338(84.2)	0	180	180	1.078	1.086	1.079
		M06	Min	0	1.2087	0.0681	0.0049(0.5)	0.0122(3.2)	0.0197(8.4)	0.0639(87.9)	0	180	0	1.438	1.337	1.557
					2.2884	0.0399	0.0048(1.4)	0.0196(24.1)	0.0043(1.2)	0.0342(73.3)	0	0	0	1.087	1.077	1.081
			TS	0.40	1.2085	0.0663	0.0047(0.5)	0.0052(0.6)	0.0186(7.9)	0.0633(91.0)	0	0	180	1.379	1.513	1.321
					2.2882	0.0362	0.0046(1.6)	0.0122(11.4)	0.0055(2.3)	0.0333(84.7)	0	180	180	1.076	1.085	1.078
		TPSSh	Min	0	1.2169	0.0702	0.0057(0.7)	0.0136(3.8)	0.0208(8.8)	0.0654(86.8)	0	180	0	1.446	1.344	1.573
					2.2977	0.0417	0.0055(1.7)	0.0217(27.1)	0.0048(1.3)	0.0348(69.8)	0	0	0	1.087	1.078	1.082
			TS	0.60	1.2164	0.0678	0.0052(0.6)	0.0054(0.6)	0.0193(8.1)	0.0646(90.7)	0	0	180	1.387	1.525	1.328
					2.2972	0.0366	0.0050(1.9)	0.0123(11.3)	0.0066(3.2)	0.0335(83.6)	0	180	180	1.078	1.086	1.079
		CAM-B3LYP	Min	0	1.2098	0.0698	0.0058(0.7)	0.0125(3.2)	0.0207(8.8)	0.0652(87.3)	0	180	0	1.440	1.336	1.562
					2.2886	0.0416	0.0055(1.7)	0.0203(23.8)	0.0037(0.8)	0.0357(73.6)	0	0	0	1.085	1.076	1.080
			TS	0.36	1.2096	0.0682	0.0056(0.7)	0.0057(0.7)	0.0199(8.5)	0.0647(90.1)	0	0	180	1.378	1.518	1.319
					2.2885	0.0378	0.0054(2.0)	0.0127(11.3)	0.0048(1.6)	0.0349(85.1)	0	180	180	1.076	1.084	1.077
		HSE06	Min	0	1.2118	0.0692	0.0053(0.6)	0.0127(3.4)	0.0197(8.1)	0.0649(87.9)	0	180	0	1.441	1.340	1.562
					2.2924	0.0410	0.0051(1.5)	0.0204(24.8)	0.0052(1.6)	0.0348(72.1)	0	0	0	1.087	1.078	1.082
			TS	0.48	1.2114	0.0672	0.0049(0.5)	0.0053(0.6)	0.0185(7.6)	0.0642(91.3)	0	0	180	1.382	1.517	1.323
					2.2920	0.0368	0.0047(1.6)	0.0120(10.6)	0.0067(3.3)	0.0338(84.4)	0	180	180	1.078	1.086	1.079
		B2PLYP	Min	0	1.2158	0.0679	0.0048(0.5)	0.0136(4.0)	0.0205(9.1)	0.0631(86.4)	0	180	0	1.444	1.346	1.568
					2.2936	0.0405	0.0045(1.2)	0.0220(29.5)	0.0043(1.1)	0.0334(68.1)	0	0	0	1.084	1.076	1.079
			TS	0.36	1.2154	0.0658	0.0044(0.4)	0.0057(0.7)	0.0194(8.7)	0.0625(90.1)	0	0	180	1.386	1.522	1.329
					2.2933	0.0358	0.0042(1.4)	0.0130(13.2)	0.0056(2.4)	0.0326(83.0)	0	180	180	1.075	1.083	1.076
2	F	B3LYP	Min	0	1.2170	0.0773	0.0055(0.5)	0.0115(2.2)	0.0137(3.1)	0.0750(94.1)	0	180	0	1.450	1.345	1.567
					2.4977	0.0761	0.0004(0.0)	0.0222(8.5)	0.0719(89.3)	0.0113(2.2)	0	0	0	1.262	1.304	1.278
			TS	0.35	1.2167	0.0761	0.0052(0.5)	0.0053(0.5)	0.0129(2.9)	0.0746(96.2)	0	0	180	1.389	1.525	1.328
					2.4974	0.0761	0.0001(0.0)	0.0158(4.3)	0.0737(93.7)	0.0107(2.0)	0	180	180	1.306	1.265	1.295
3	Cl	B3LYP	Min	0	1.2174	0.0623	0.0055(0.8)	0.0090(2.1)	0.0161(6.7)	0.0593(90.5)	0	180	0	1.449	1.355	1.548
					2.8885	0.0572	0.0049(0.7)	0.0171(8.9)	0.0499(76.2)	0.0215(14.1)	0	0	0	1.646	1.697	1.662
			TS	0.27	1.2171	0.0609	0.0052(0.7)	0.0040(0.4)	0.0153(6.3)	0.0586(92.5)	0	0	180	1.395	1.513	1.340
					2.8882	0.0570	0.0046(0.7)	0.0143(6.3)	0.0509(79.7)	0.0208(13.3)	0	180	180	1.699	1.649	1.684
4	Br	B3LYP	Min	0	1.2162	0.0594	0.0054(0.8)	0.0082(1.9)	0.0157(7.0)	0.0564(90.3)	0	180	0	1.447	1.357	1.541
					3.0485	0.0537	0.0056(1.1)	0.0154(8.2)	0.0433(65.0)	0.0272(25.7)	0	0	0	1.806	1.859	1.822
			TS	0.22	1.2158	0.0580	0.0050(0.7)	0.0037(0.4)	0.0150(6.7)	0.0557(92.2)	0	0	180	1.395	1.508	1.342
					3.0482	0.0532	0.0053(1.0)	0.0130(6.0)	0.0439(68.2)	0.0265(24.8)	0	180	180	1.862	1.809	1.844
5	I	B3LYP	Min	0	1.2173	0.0547	0.0053(0.9)	0.0070(1.6)	0.0155(8.0)	0.0517(89.4)	0	180	0	1.449	1.362	1.534
					3.2658	0.0493	0.0067(1.8)	0.0122(6.1)	0.0321(42.4)	0.0347(49.6)	0	0	0	2.022	2.075	2.036
			TS	0.14	1.2170	0.0534	0.0050(0.9)	0.0032(0.4)	0.0150(7.9)	0.0509(90.9)	0	0	180	1.399	1.504	1.348
					3.2655	0.0484	0.0064(1.7)	0.0101(4.4)	0.0322(44.3)	0.0341(49.6)	0	180	180	2.080	2.024	2.058

[a] Energy values in kcal/mol relative to the minimum (Min) of the BPR surface; breathing radii R and R^S, total deformation amplitudes T and T^S, deformation amplitudes t_n and t_n^S in Å; deformation phase angles in deg; CC and CX bond lengths all in Å. The second line gives the deformation coordinates of the virtual substituent ring X_5 and the CX bond lengths.

Table 4. RB3LYP and REKS(2,2)/B3LYP/(SDB-)cc-pVTZ results for pentahalogeno CPCs $C_5X_5^+$.[a]

X	State	Sym.	Comment	ΔE	ZPE	$\Delta H(298)$	$\Delta G(298)$	S	CC	CX
H	$\tilde{X}^3A_2'$	D_{5h}	Ground state	−8.59	50.61	−7.82	−7.17	63.96	1.4203	1.0794
	$^1E_2'$	D_{5h}	First excited state	7.69	48.69	6.69	7.65	62.90	1.4221	1.0793
	$^1A_1$	C_{2v}	TS of BPR	0.54	49.17	0.00	0.00	66.14	1.4284	1.0799
	$^1A_1$	C_{2v}	Min of BPR	0.00	49.88	0.29	0.18	66.50	1.4291	1.0799
F	$\tilde{X}^3A_2'$	D_{5h}	Ground state	−5.07	26.71	−4.42	−4.01	86.99	1.4229	1.2860
	$^1E_2'$	D_{5h}	First excited state	9.87	24.77	8.15	9.70	83.20	1.4242	1.2858
	$^1A_1$	C_{2v}	TS of BPR	0.35	25.83	0.00	0.13	87.94	1.4314	1.2851
	$^1A_1$	C_{2v}	Min of BPR	0.00	26.29	0.42	0.00	89.80	1.4311	1.2851
Cl	$\tilde{X}^3A_2'$	D_{5h}	Ground state	−5.59	21.75	−4.70	−4.44	99.00	1.4243	1.6722
	$^1E_2'$	D_{5h}	First excited state	5.30	19.95	4.50	4.72	99.16	1.4247	1.6716
	$^1A_1$	C_{2v}	TS of BPR	0.27	20.73	0.00	0.07	99.64	1.4315	1.6727
	$^1A_1$	C_{2v}	Min of BPR	0.00	21.22	0.54	0.00	101.69	1.4310	1.6728
Br	$\tilde{X}^3A_2'$	D_{5h}	Ground state	−6.07	19.49	−5.13	−4.88	112.54	1.4233	1.8325
	$^1E_2'$	D_{5h}	First excited state	4.14	17.70	3.45	3.59	112.90	1.4233	1.8321
	$^1A_1$	C_{2v}	TS of BPR	0.22	18.53	0.00	0.21	112.68	1.4300	1.8334
	$^1A_1$	C_{2v}	Min of BPR	0.00	18.96	0.58	0.00	115.35	1.4295	1.8335
I	$\tilde{X}^3A_2'$	D_{5h}	Ground state	−5.37	18.03	−4.37	−4.10	122.12	1.4253	2.0476
	$^1E_2'$	D_{5h}	First excited state	3.18	16.38	2.61	3.14	121.26	1.4248	2.0471
	$^1A_1$	C_{2v}	TS of BPR	0.14	17.14	0.00	0.38	121.78	1.4312	2.0490
	$^1A_1$	C_{2v}	Min of BPR	0.00	17.47	0.60	0.00	125.08	1.4308	2.0490

[a] Low symmetry forms are calculated with restricted B3LYP, the high symmetry forms with REKS(2,2)/B3LYP. Energy values in kcal/mol relative to the minimum (Min) of the BPR surface; entropy S in entropy units; breathing radii R and R^S, total deformation amplitudes T and T^S, CC and CX bond lengths all in Å. In the case of C_{2v}-symmetry, average CC and CH bond lengths are given.

valley surrounding the central area of the singlet surface (Figs. 3 and 4). The various forms of CPC populating the BPR valley can be described at the single determinant level as can be confirmed by an inspection of the data listed in Table 4.

Bond pseudorotation of CPC

The Jahn–Teller distortion of **1c** leads to the $^1A_1$ and $^1B_2$ states. Borden and Davidson[12] showed that the (linear) JTE of CPC is weak and that the actual distortion of the D_{5h} form is caused by the vibronic coupling of the $^1E_2'$ state via an E_2'' vibration to the $^1A_1'$ state of the same electronic configuration (PJTE). Recently, Wörner and Merkt[9] have investigated CPC **1** by combining PFI-ZEKE photoelectron spectroscopy and ab initio calculations. After an elaborate and complicated analysis of the JTE and PJTE, these authors come to the conclusion that the $^1E_2'$ state is subject to a "very weak linear JTE and an unusually strong PJTE".

As discussed in Computational Methods Section, there are three elementary BPR cycles with $n = 1, 2, 3$ (Fig. 2) that can contribute to the actual BPR process of **1a**. Their contributions (in %, Table 3) are reflected by the magnitude of the corresponding displacement amplitudes t_n in relation to the total deformation amplitude T according to Eq. (10). Parameter T gives the magnitude of C_5 deformation and thereby represents a measure for the stabilization of the five-ring relative to its D_{5h}-symmetrical form in the $^1E_2'$ state. As revealed by the deformation coordinates listed in Table 3, the calculated T values are all close to 0.06 ± 0.01 Å, where the T value of the dienylic form **1a** is always larger (up to 20%, Table 2) than that of the allylic form **1b**. This indicates that the deformation of **1c** to **1a** is easier and accordingly **1a** experiences a somewhat larger stabilization thus making it the minimum energy form of the deformation surface.

The difference in the T values follows the trends found for the calculated t_3 amplitudes, which dominate the ring deformation with contributions of 90% (MRAQCC values, Table 3) for the dienylic minima at 0, 72, 144, 216, and 288°, and 77% for the allylic TSs at 36, 108, 180, 252, and 324° (Figs. 4 and 5). Deformation mode $n = 3$, which by its nature is the most delocalized one involves all ring bonds and accordingly facilitates a dynamic deformation. At all levels of theory used, the energy barrier to BPR is smaller than 1 kcal/mol, where the MRAQCC value of 0.35 kcal/mol is probably the most accurate one. Despite this small energy difference, all methods agree in predicting the major geometric and energetic features of dienylic and allylic forms **1a** and **1b**. This is in line with the results of previous publications on CPC **1**.[9, 12–14]

One may be tempted to explain the slightly larger stability of **1a** in terms of electron delocalization, antiaromaticity, ring strain, CC bond strength, charge distribution, or CH bond interactions. None of these approaches leads to a simple explanation of the stability difference. The alternative and much more convincing explanation is that a slightly larger T enabled by the larger flexibility of the dienylic form **1a** leads to a somewhat larger deformation stabilization. This effect could of course be outweighed by stronger substituent interactions, which obviously is not the fact for X = H.

For CPC, the linear Jahn–Teller space is 6D, spanned by three E_1' vibrational normal coordinate pairs identified and described in Table 1. These are associated with a degenerate ring deformation vibration (elementary BPR process with $n = 1$), a degenerate CCH bending mode (corresponding to the deformation mode $n = 1$ for the virtual H_5 ring) and a degenerate CH stretching mode caused by the $\{T_x - T_x, T_y - T_y\}$-couplings (Table 1). The latter makes only a small contribution to the Jahn–Teller space

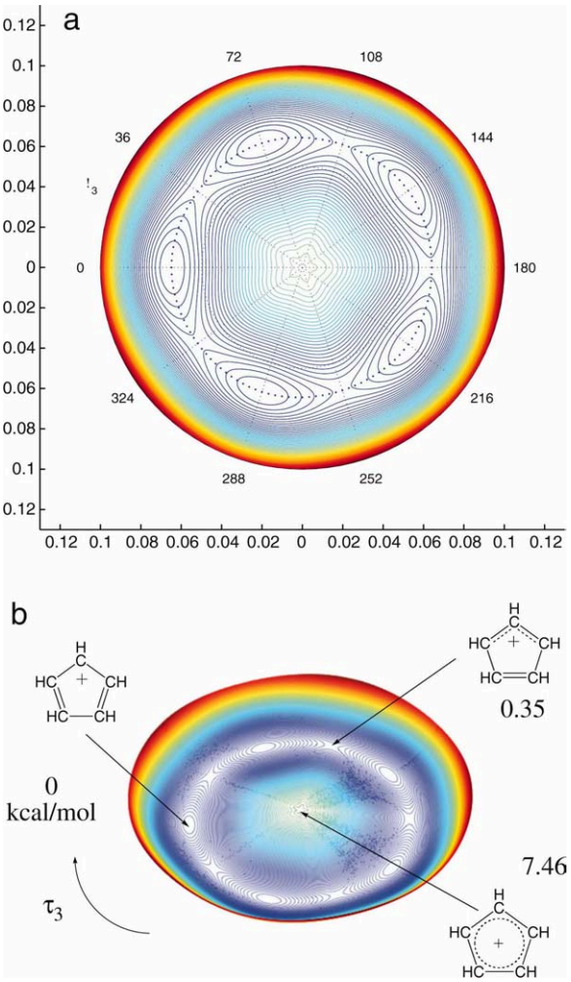

Figure 4. **a**) Contourline diagram and **b**) perspective drawing of the BPR energy surface of the CPC calculated at the MRAQCC(4,5)/cc-pVTZ level of theory. The radial deformation coordinate is amplitude t_3 (given in **a**) in the vertical and horizontal direction) and the angular coordinate phase angle τ_3. The five minima occupied by the dienylic forms are at τ_3 = 0, 72, 144, 216, and 288° and the first-order transition states occupied by the allylic forms at 36, 108, 180, 252, and 324°. [Color figure can be viewed in the online issue, which is available at wileyonlinelibrary.com.]

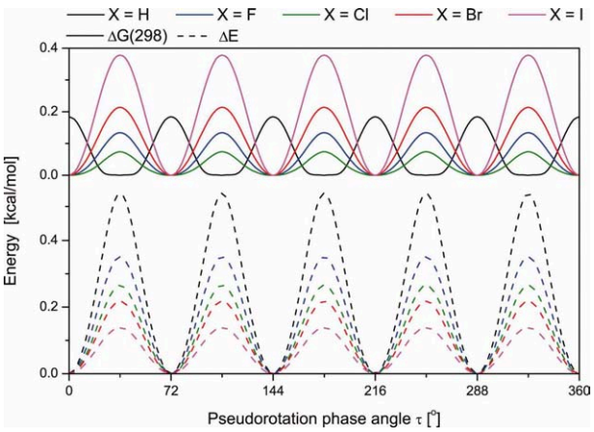

Figure 5. Changes in the potential along the BPR path of the CPCs $C_5X_5^+$. Dashed lines (lower part): changes in the energy ΔE. Solid lines (upper part): changes in the free energy $\Delta G(298)$. B3LYP/cc-pVTZ or B3LYP/SDB-cc-pVTZ calculations for X = H, F, Cl, Br, I.

($\Delta t = 0.0096$ Å for **1a** and 0.0095 Å for **1b**; substituent positions determined using the four t_n^S-values of Table 3 agree with those obtained in the geometry optimization with an accuracy better than 0.01 Å). We find that of the three degenerate modes only the CCH bending mode contributes to the Jahn–Teller space as is reflected by a 32% (31 %) contribution for **1a** (**1b**) to the total ring deformation. Hence, the linear Jahn–Teller deformation of the $^1E_2'$ state is, according to the calculated deformation coordinates, small and results mainly from E_1'-symmetrical CCH bending.

The four E_2' vibrational modes that span an 8D PJTE space cause the major part of the $C_5X_5^+$ deformation from D_{5h} to either C_{2v} or C_s symmetry. These are the two degenerate C_5 deformation modes associated with $n = 2, 3$, the degenerate CH stretching mode associated with $\{t_2^S,\tau_2^S\}$ and the degenerate CCH bending mode associated with $\{t_3^S,\tau_3^S\}$. For minimum **1a**, the largest contributions result from t_3 (89%) and t_3^S (63%), which means that the PJTE clearly dominates the deformation of CPC **1c**. For TS **1b**, there is in addition to the t_3 (77%) and t_3^S (63%) contributions also a t_2 contribution of 20% (Table 3). Inspection of Figure 2 reveals that the latter contribution is necessary because all forms with τ_3 being equal to 36, 108, 180, 252, or 324° possess just one short CC bond opposite to an acute CCC angle, which leads to a strained allylic unit. However, an admixture of τ_2-forms with 0, 72, 144, 216, or 288° helps to widen the CCC angle and to stabilize the allylic unit.

All mode 2 and 3 deformations (Fig. 2) take place in the PJTE space, which underlines that the PJTE clearly dominates the deformation of **1c**. This conclusion results from a simple inspection of the calculated curvilinear deformation coordinates of Table 3 and is in line with the vibronic coupling analysis (see e.g., Wörner and Merkt[9]). It has to be noted that at all levels of theory, the breathing deformation makes a very small contribution to the deformation of the D_{5h} ring, which agrees with the fact that the average CC bond length (Table 2) increases by just 0.005 Å suggesting some slight destabilization, which of course is outweighed by the PJTE.

The contourline diagram and perspective drawing of Figure 4 depict the BPR surface in the t_3, τ_3-space, as it was drawn from the analytic function shown in Table 4 [see also Eq. (11)]. BPR implies that the positive charge (Fig. 3) moves along the perimeter of the ring as do all CC bonds or fragments (the allylic or dienylic fragment) without leading to an angular momentum. The 10 forms shown in Figure 3 are located at the 10 stationary points of the BPR path. Apart from these forms, there is an infinite number of CPC forms located along the BPR path with energy differences being less than 0.35 kcal/mol (MRAQCC result, Tables 2 and 3). It has to be noted that for all levels calculated the $\Delta G(298)$ values favor the allylic forms for similar reasons as already discussed in the case of the MRAQCC results.

Bond pseudorotation of perhalogenated CPC

The global features of the deformation surfaces of perhalogenated CPCs **2**–**5** are similar to those of the parent ion as can

Table 5. Coefficients of the BPR potential calculated at B3LYP/(SDB-)cc-pVTZ.[a]

	$C_5H_5^+$	$C_5F_5^+$	$C_5Cl_5^+$	$C_5Br_5^+$	$C_5I_5^+$
V_{2000}	6426.82	8243.83	7212.16	6151.79	6503.13
V_{4000}	2111352.08	−1502072.38	9343814.03	9798312.14	5409970.95
V_{0200}	−18740.38	−35667.75	−23710.68	−20117.01	−16247.67
V_{0400}	15133157.01	41534083.27	32904354.47	30842956.90	27453275.60
V_{0020}	−1789.12	−2408.10	−1373.76	−1119.86	−990.94
V_{0040}	136035.82	164406.36	117349.30	107909.35	127673.88
V_{2200}	−10913016.29	−2358033.69	−22002868.50	−20175407.29	−17140453.23
V_{2020}	−517505.74	−1249715.41	−991470.59	−925200.50	−1111721.08
V_{0220}	1663991.03	3775367.28	2457588.00	2032842.47	1512359.95
V_{1005}	−0.69	−8.61	8.35	7.32	0.79
V_{0105}	5.08	23.23	6.68	6.21	4.53
V_{0015}	−2.73	2.26	−0.98	−0.62	−0.05

[a] The high symmetry forms were calculated with REKS(2,2)/B3LYP. For the explanation of the potential coefficients V, see text and Eq. (11). Deviation from B3LYP calculated relative energies is smaller than 0.05 kcal/mol.

be confirmed by inspection of the analytic deformation surfaces given in Table 5. Calculated BPR barriers for **2** (X = F), **3** (X = Cl), **4** (X = Br), and **5** (X = I) decrease from 0.26 to 0.14 kcal/mol (Table 3) where in all cases the dienylic form is more stable than the allylic form for reasons, which are discussed above. The decrease in the energy barriers can be directly related to a decrease in the deformation amplitudes T and t_3 (Table 3). These trends are a result of the increasing volume of the halogen substituents with increasing atomic number. Exchange repulsion between the halogen atoms makes the ring stiffer so that the ring deformation is sterically limited and a lower deformation stabilization results. This trend is directly reflected in the relative energies of the $^1E_2'$ state for **2**–**5** (REKS(2,2)/B3LYP/cc-pVTZ: 9.9; 5.3; 4.1; 3.2 kcal/mol compared to 7.7 kcal/mol for X = H; Table 4) as well as the corresponding singlet–triplet splitting (14.9; 10.9; 10.2; 8.6 kcal/mol compared to 16.3 kcal/mol for X = H, Table 4), where, however, the absolute values of these quantities may be too large by 1–2 kcal/mol considering the incomplete description of the multireference character of the $^1E_2'$ state at REKS-DFT or other methods with limited active space and/or lack of infinite order correlation effects.

In the case of the parent CPC **1**, the central barrier is just 7.5 kcal/mol (Table 2), which is reduced by almost 60% in the case of **5** (to 3.2 kcal/mol, Table 4). Although we could not obtain MRAQCC values for the $^1E_2'$ state of $C_5X_5^+$ (X ≠ H) because of calculational limitations, we predict that **5** in its first excited singlet state can cross the region of the conical intersection in the center of the deformation surface (t_n = 0 for all n) and in this way undergo ring inversion (conversion from $\tau = 0$ to $\tau = 180°$ via the D_{5h} form) or get to another excited state. However, the investigation of these possible processes was outside the scope of this work.

The calculated trends in curvilinear deformation coordinates indicate that the influence of the halogen substituents in $C_5X_5^+$ plays a larger role than that of the H atoms in the parent molecule. Halogens, when bonded to a positively charged C atom, can establish partial double bonds by π-donation to the C atom.[48] This makes CCX bending more difficult and thereby reduces t_1^S, whereas the t_2^S contribution (CX length changes) becomes larger. This means that the influence of the JTE is more decreased and that of the PJTE more increased compared to the parent ion. For X = F, electrostatic repulsion between the X atoms and partial CX double bond character is most developed thus leading to a stronger CF stretching deformation (t_2^S close to 90%, Table 3; also $\Delta t = 0.0136$ Å for the dienylic form because of a short C1F1 bond) and almost no CCF bending deformation (t_3^S close to 2%, Table 3). For X = I, electrostatic repulsion is reduced as is the CX double bond character. Consequently, values of t_2^S and t_3^S approach each other (both close to a 50% contribution, Table 3; also $\Delta t = 0.0095$ Å for the dienylic form because of a less shortened C1I1 bond; a large Δt means that the virtual X5 ring is shifted along the C1X1 direction for $\tau = 0$ so that the bond C1X1 becomes shorter).

CCSD(T)/(SDB-)cc-pVTZ calculations predict BPR barriers of 0.02, 0., 0.01, and 0.02 kcal/mol thus describing all perhalogenated CPC molecules energetically as free pseudorotors. This is in line with deformation amplitudes T and T^S (Table 3) along the BPR path that vary by 10^{-3} Å or less. However, vibrational, thermochemical, and entropic corrections add another 0.3–0.5 kcal/mol to the BPR barrier (see also Fig. 5).

Conclusions

In this work, the dynamic process of BPR has been investigated for CPC **1** and the four pentahalogeno CPC molecules **2**–**5** for the first time. MRAQCC(4,5) calculations of the parent ion reveal that the singlet–triplet splitting between the D_{5h}-symmetrical X^3A_2' ground state and the D_{5h}-symmetrical $^1E_2'$ first excited state can be reliably described to be 14.35 kcal/mol with a $\Delta G(298)$ value of 12.85 kcal/mol, whereas the adiabatic splitting is just 6.89 and 4.54 kcal/mol. The latter value is in close agreement with the experimental value of 4.38 kcal/mol.[9] The D_{5h}-symmetrical $^1E_2'$ state deforms to a C_{2v}-symmetrical $^1A_1$ state, which is 7.46 kcal/mol lower in energy. The $^1A_1$ state can undergo free BPR at room temperature ($\Delta G(298) = 0.05$ kcal/mol). The MRAQCC energy barrier is just 0.35 kcal/mol, which is reduced to a negligible value by vibrational and entropic effects. For all CPCs investigated, the dienylic forms are energetically slightly

favored compared to the allylic forms at the TSs of the BPR surface.

The deformation space of the CPC molecules $C_5X_5^+$ is 17D (7D for the C_5 ring, 7D for the virtual X_5 ring, plus a 3D coupling space), which contains the 6D linear Jahn–Teller deformation space and the 8D pseudo-Jahn–Teller space beside three 1D spaces. The deformation analysis in terms of curvilinear coordinates reveals that the linear JTE is small and preferentially caused by the E_1'-symmetrical CCH bending associated with curvilinear coordinates $\{t_1^S, \tau_1^S\}$. There is a strong pseudo-Jahn–Teller deformation associated with the E_2'-symmetrical ring distortion mode represented by $\{t_3, \tau_3\}$ and the E_2'-symmetrical CCH bending mode represented by $\{t_3^S, \tau_3^S\}$. The PJTE is more stabilizing in the dienylic forms as reflected by the total deformation amplitudes T. The admixture of the E_2'-symmetrical deformation mode represented by $\{t_2, \tau_2\}$ with $\tau_2 = 0°$ in the case of the TSs reveals the necessity of adjusting the angle C2C1C5 in the allylic part (see Fig. 2). Vibrational effects revert the order of stability, whereas entropic effects almost change it back.

Perhalogenation of CPC does not lead to a change in the relative stability of dienylic and allylic CPC forms. However, the C_5 ring becomes stiffer. This is a result of forming partial $C = X$ double bonds and the electrostatic repulsion between the X atoms. The total deformation as quantitatively assessed by the total deformation amplitude T decreases and thereby the deformation stabilization of CPC becomes smaller. This is confirmed by the trend in the calculated stabilization energies resulting from ring deformation, which are reduced from 7.7 (X = H) to 3.2 kcal/mol (X = I) according to REKS(2,2) calculations (Table 4). Perhalogenation leads to a further reduction of the linear JTE so that deformation is predominantly a result of a stabilizing PJTE.

In early work on CPC and its derivatives, one emphasized the 4π electron configuration of the ion and concluded that the molecular properties of CPC are a result of its inherent antiaromaticity. This work strongly suggests that the PJTE determines the properties of the lowest singlet state of CPC and its derivatives. The static concept of antiaromaticity based on the π-MOs and the corresponding π-electron configuration does not lead to a thorough explanation of the properties of CPCs. The properties of CPC ions are the result of the in-plane rotations of the 5 C nuclei around the corners of a pentagon, which lead, because these rotations are coupled, to the dynamic process of (at room temperature unhindered) BPR as described in this work.

The use of curvilinear deformation coordinates provides an easy way of assessing the relative importance of JTE and PJTE and identifying their dominant contributions in a multidimensional space.

Acknowledgment

The authors thank SMU for providing computational resources.

Keywords: bondpseudorotation • Jahn–Teller effect • pseudo-Jahn–Teller effect • cyopentadienyl cation • deformation coordinates

How to cite this article: W. Zou and D. Cremer, *Int. J. Quantum Chem.* **2012**, DOI: 10.1002/qua.24116

[1] A. D. Liehr, *J. Phys. Chem.* **1963**, *67*, 389.
[2] A. D. Liehr, *J. Phys. Chem.* **1963**, *67*, 472.
[3] I. B. Bersuker, *The Jahn-Teller Effect*, Cambridge University Press: Cambridge, 2006.
[4] D. Cremer, E. Kraka, K. J. Szabo, In *The Chemistry of Functional Groups, The Chemistry of the Cyclopropyl Group, Vol. 2*, Z. Rappoport, Ed.; John Wiley: New York, 1995, p. 43.
[5] W. Zou, D. Izotov, D. Cremer, *J. Phys. Chem.* **2011**, *115*, 8731.
[6] M. Saunders, R. Berger, A. Jaffe, *J. Am. Chem. Soc.* **1973**, *95*, 3017.
[7] E. Wasserman, R. S. Hutton, *Acc. Chem. Res.* **1977**, *10*, 27.
[8] H. J. Wörner, F. Merkt, *Angew. Chem., Int. Ed.* **2006**, *45*, 293.
[9] H. J. Wörner, F. Merkt, *J. Chem. Phys.* **2007**, *127*, 034303.
[10] W. J. Hehre, P. Schleyer, *J. Am. Chem. Soc.* **1973**, *95*, 5837.
[11] B. Glukhovtsev, M. N. Reindl, P. Schleyer, *Mendeleev Commun.* **1993**, *3*, 100.
[12] W. T. Borden, E. R. Davidson, *J. Am. Chem. Soc.* **1979**, *101*, 3771.
[13] E. P. F. Lee, T. G. Wright, *Phys. Chem. Chem. Phys.* **1999**, *1*, 219.
[14] S. Zilberg, Y. Haas, *J. Am. Chem. Soc.* **2002**, *124*, 10683.
[15] F. P. Lossing, J. C. Traeger, *J. Am. Chem. Soc.* **1975**, *97*, 1579.
[16] H. Schwarz, H. Thies, W. Franke, In *Ionic Processes in the Gas Phase*, F. M. A. A. eds.; Reidel: Dordrecht, 1984, p. 267.
[17] M. Allen, A. D. Sumonja, T. T. Tidwell, *J. Am. Chem. Soc.* **1997**, *119*, 2371.
[18] D. Cremer, J. A. Pople, *J. Am. Chem. Soc.* **1975**, *97*, 1354.
[19] D. Cremer, *J. Phys. Chem.* **1990**, *94*, 5502.
[20] D. Cremer, K. J. Szabo, In *Methods in Stereochemical Analysis, Conformational Behavior of Six-Membered Rings, Analysis, Dynamics, and Stereoelectronic Effects*, E. Juaristi, Ed.; VCH Publishers, New York, 1995, p. 59.
[21] W. Zou, D. Cremer, *J. Chem. Phys.* **2011**, paper is submitted.
[22] D. Cremer, D. Izotov, W. Zou, E. Kraka, *RING, A Coordinate Transformation Program* 2011, Southern Methodist University, Dallas, TX.
[23] E. Kraka, D. Cremer, M. Filatov, W. Zou, J. Gräfenstein, D. Izotov, J. Gauss, Y. He, A. Wu, V. Polo, L. Olsson, Z. Konkoli, Z. He, *COLOGNE2011* (2011), Southern Methodist University, Dallas, TX.
[24] J. F. Stanton, J. Gauss, M. E. Harding, P. G. Szalay, A. A. Auer, R. J. Bartlett, U. Benedikt, C. Berger, D. E. Bernholdt, Y. J. Bomble, L. Cheng, O. Christiansen, M. Heckert, O. Heun, C. Huber, T.-C. Jagau, D. Jonsson, J. Jusélius, K. Klein, W. J. Lauderdale, D. A. Matthews, T. Metzroth, L. A. Mück, D. P. O'Neill, D. R. Price, E. Prochnow, C. Puzzarini, K. Ruud, F. Schiffmann, W. Schwalbach, S. Stopkowicz, A. Tajti, J. Vázquez, F. Wang, J.D. Watts, J. Almlöf, P. R. Taylor, T. Helgaker, H. J. Aa. Jensen, P. Jørgensen, J. Olsen, A. V. Mitin, C. van Wüllen, *CFOUR, a Quantum Chemical Program Package* (2010), see http://www.cfour.de. (Accessed on January 15, 2012).
[25] H. J. Werner, P. J. Knowles, G. Kniza, F. R. Manby, M. Schütz, P. Celani, T. Korona, R. Lindh, A. Mitrushenkov, G. Rauhut, K. R. Shamasundar, T. B. Adler, R. D. Amos, A. Bernhardsson, A. Berning, D. L. Cooper, M. J. O. Deegan, A. J. Dobbyn, F. Eckert, E. Goll, C. Hampel, A. Hesselmann, G. Hetzer, T. Hrenar, G. Jansen, C. Köppl, Y. Liu, A. W. Lloyd, R. A. Mata, A. J. May, S. J. McNicholas, W. Meyer, M. E. Mura, A. Nicklass, D. P. O'Neill, P. Palmieri, K. Pflüger, R. Pitzer, M. Reiher, T. Shiozaki, H. Stoll, A. J. Stone, R. Tarroni, T. Thorsteinsson, M. Wang, A. Wolf, *MOLPRO, Version 2010.1, A Package of Ab initio Programs*, 2010, see http://www.molpro.net. (Accessed on January 15, 2012).
[26] P. G. Szalay, R. J. Bartlett, *Chem. Phys. Lett.* **1993**, *214*, 481.
[27] K. Raghavachari, G. W. Trucks, J. A. Pople, M. Head-Gordon, *Chem. Phys. Lett.* **1989**, *157*, 479.
[28] H.-J. Werner, P. J. Knowles, *J. Chem. Phys.* **1985**, *82*, 5053.
[29] P. J. Knowles, H.-J. Werner, *Chem. Phys. Lett.* **1985**, *115*, 259.
[30] H.-J. Werner, *Mol. Phys.* **1996**, *89*, 645.
[31] A. D. Becke, *J. Chem. Phys.* **1993**, *98*, 5648.

[32] P. J. Stevens, F. J. Devlin, C. F. Chablowski, M. J. Frisch, *J. Phys. Chem.* **1994**, *98*, 11623.

[33] C. Adamo, V. Barone, *J. Chem. Phys.* **1999**, *110*, 6158.

[34] Y. Zhao, D. G. Truhlar, *J. Chem. Phys.* **2006**, *125*, 194101.

[35] J. M. Tao, J. P. Perdew, V. N. Staroverov, G. E. Scuseria, *Phys. Rev. Lett.* **2003**, *91*, 146401.

[36] D. Yanai, T. Tew, N. Handy, *Chem. Phys. Lett.* **2004**, *393*, 51.

[37] A. V. Krukau, O. A. Vydrov, A. F. Izmaylov, G. E. Scuseria, *J. Chem. Phys.* **2006**, *125*, 224106.

[38] S. Grimme, *J. Chem. Phys.* **2006**, *124*, 034108.

[39] M. Filatov, S. Shaik, *Chem. Phys. Lett.* **1999**, *304*, 429.

[40] M. Filatov, S. Shaik, *Chem. Phys. Lett.* **2000**, *332*, 409.

[41] D. Cremer, *Mol. Phys.* **2001**, *99*, 1899.

[42] V. Polo, J. Grafenstein, E. Kraka, D. Cremer, *Chem. Phys. Lett.* **2002**, *352*, 469.

[43] V. Polo, E. Kraka, D. Cremer, *Theor. Chem. Acc.* **2002**, *107*, 291.

[44] T. H. Dunning, *J. Chem. Phys.* **1989**, *90*, 1007.

[45] J. M. L. Martin, A. Sundermann, *J. Chem. Phys.* **2001**, *114*, 3408.

[46] A. Bergner, M. Dolg, W. Kuechle, H. Stoll, H. Preuss, *Mol. Phys.* **1993**, *80*, 1431.

[47] H. Köppel, W. Domcke, L. S. Cederbaum, *Adv. Chem. Phys.* **1984**, *57*, 59.

[48] E. Kraka, D. Cremer, *Chem. Phys. Chem.* **2009**, *10*, 686.

Received: 30 January 2012
Revised: 1 March 2012
Accepted: 5 March 2012
Published online on Wiley Online Library